THE JOURNAL OF PHYSICAL CHEMISTRY C

Article

pubs.acs.org/JPCC

Block Copolymers Self-Assembly Allows Obtaining Tunable Micro or Nanoporous Membranes or Depth Filters Based on PMMA; Fabrication Method and Nanostructures

Javier Pinto,*[,†,‡,§] Michel Dumon,[‡,§] Miguel A. Rodriguez-Perez,*[,†] Ricardo Garcia,[∥] and Christian Dietz[⊥]

[†]CellMat Laboratory, Condensed Matter Physics Department, University of Valladolid, Paseo de Belen no. 7, 47001 Valladolid, Spain

[‡]Laboratoire de Chimie des Polymères Organiques (LCPO), Universite Bordeaux, LCPO, UMR 5629, F-33600 Pessac, France

[§]CNRS, LCPO, UMR 5629, F-33600 Pessac, France

[∥]Instituto de Ciencia de Materiales de Madrid, CSIC, C/Sor Juana Inés de la Cruz no. 3, 28049 Madrid, Spain

[⊥]Center of Smart Interfaces and Department of Materials Science, Technische Universität Darmstadt, Alaric-Weiss-Strasse 2, 64287 Darmstadt, Germany

ABSTRACT: An environmentally friendly method to produce tunable bulk micro or nanoporous structures is presented. Nano- and micro-porous structures are obtained by gas dissolution foaming using CO_2, following the pattern of polymer blends between poly(methylmethacrylate) (PMMA) and a triblock copolymer, namely poly(methylmethacrylate)-*co*-poly(butyl acrylate)-*co*-poly(methyl methacrylate) (MAM) blends nanostructuration. Membranes or depth filters can be produced by this method, varying the amount of the triblock copolymer in the blend. Furthermore, main characteristics, such as the average pore size and porosity can be finely tuned by adjusting the process parameters (temperature or pressure) during gas foaming.

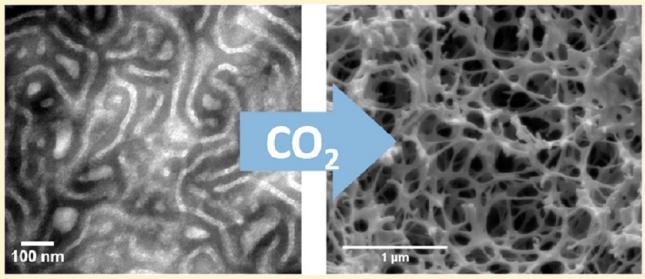

1. INTRODUCTION

Nowadays, particle filters are being used in a wide range of industrial applications, such as wastewater treatment, particles or biological samples collection, and desalination, among others.[1,2] Filtration processes and their potential applications can be classified by the size of the particles that could be separated, related to the pore size of the porous material. Particles with sizes higher than 1 μm can be separated by usual particle filtration, from sizes of 50 to 500 nm the separation process is called microfiltration, for particles between 2 and 50 nm ultrafiltration filters are required, and lower particle sizes than 2 nm could be separated by nanofiltration.[3] Filters can also be classified by their thickness. On the one hand, depth filters have a significant physical depth and the particles to be retained are captured throughout the depth of the filter. Depth filters often have a labyrinthine three-dimensional structure, with multiple channels and heavy branching (high tortuous path), so that there is a large pathway through which the liquid must flow and by which the filter can retain particles.[4] On the other hand, membrane filters are porous media in which depth is not considered important. The membrane filter uses a relatively thin material with a well-defined maximum pore size, and the particle retaining effect takes place almost entirely at the surface. Membranes offer the advantage of having well-defined effective pore sizes, can be integrity tested more easily than depth filters, and can achieve filtration of smaller particles.[5]

Development of filters based on polymers has acquired relevance in recent years, mainly in microfiltration and ultrafiltration processes. Focusing on the microfiltration, several fabrication methods to produce polymeric filters can be found in the literature: predefined patterns were transferred into a polymer film by lithographic and pattern-transfer techniques;[6,7] track etch technique can produce nanoporous membranes by irradiating polymers with high energy particles;[7,8] natural formation of nanostructured polymers via precipitation allows the use of solvent-based procedures;[9,10] biologically derived structures could act as porous membranes;[11,12] and in addition, nanoporous materials could also be obtained from self-assembly of block copolymers by the selective removal of one of the blocks.[7,13−16] Nanoporous structure templating from block copolymer morphologies has been studied since the 1995s on films (≪1 mm) of generally high-Tg polymers by thermal degradation of one part of the polymer/copolymer, or in other polymers by solvent effects or organization of surfactants.[7,13,14,17,18] Moreover, block copolymers have been used as structure-directing agents in the production of silica membranes by evaporation-induced self-assembly.[19]

Some attempts to use foaming process with supercritical CO_2 could be found in the literature with polymeric thin films,[20,21] but not on bulk samples. In general, each production route allows us to obtain just one kind of filter, membrane, or depth filter, and

Received: October 2, 2013
Revised: February 1, 2014
Published: February 6, 2014

   dx.doi.org/10.1021/jp409803u | *J. Phys. Chem. C* 2014, 118, 4656−4663

requires the fabrication of different patterns to control the pore size.

In previous works, micro and nanoporous structures based on the self-assembly of block copolymers (MAM, SBM) in polymer blends were obtained using a different approach (for the pore generation) from those described above,[22,23] called gas solid state foaming technique, with CO_2 as the physical foaming agent.[23] This technique exhibits several advantages: it is industrially scalable and environmental friendly.[25,26] In this work, we prove that by an appropriate selection of PMMA/MAM blends and of process parameters, it is possible to produce nanoporous membranes and depth filters with tunable pore size, using the gas solid state foaming technique, with the additional advantage of the proven biocompatibility of PMMA.[27,28] In addition to this, a detailed study of the morphology of the initial dense precursors and the nanoporous structure of the filters is also presented.

2. EXPERIMENTAL SECTION

2.1. Materials. Transparent poly(methyl methacrylate) (PMMA) and poly(methyl methacrylate)-*co*-poly(butyl acrylate)-*co*-poly(methyl methacrylate) (MAM) were kindly supplied by the Arkema Company (France), in the form of pellets. PMMA homopolymer presents a glass transition temperature (T_g) of 112 °C and density of 1.18 g/cm^3. MAM triblock copolymer presents a density of 1.08 g/cm^3. Details of production of MAM copolymer can be found elsewhere.[29,30]

The particular MAM in our study, 36 wt % poly(butyl acrylate) (PBA), has the following characteristics, given by Arkema, $M_n^{MAM} \approx 85\,000$ g/mol (own SEC measurement at 85 000g/mol), $M_w^{MAM} \approx 180\,000$ g/mol (our own measure is at 165 000 g/mol), therefore $I_p^{MAM} \approx 2.1$.

The PMMA used is pure homopolymer (without impact modifier), with the following characteristics $M_w \approx 83\,000$ g/mol, $M_n \approx 43\,000$ g/mol, $I_p \approx 1.9$.

2.2. Fabrication of Solid Samples. Blends of PMMA and different amounts of MAM have been produced by the following route. First, both materials, PMMA and MAM, were dried in vacuum (680 mmHg) at 80 °C during 4 h. Then, blends with the appropriate amount of each polymer were produced by extrusion using a Scamex CE02 single screw extruder ($L/D = 28$ $d = 45$ mm), with a temperature profile from 165 to 225 °C, at a screw speed of 60 rpm. Pellets from the produced blends were obtained using a continuous cutting machine operating at the end of the extrusion line.

In a second step, produced blends in the form of pellets were dried again, in the same conditions as the raw materials. Dry blends were injected into pieces (50 × 15 mm^2) with 3 mm thickness, using a small scale injection molding machine developed by DSM Xplore. Melt temperature was fixed at 240 °C, whereas mold temperature was set at 60 °C. The injection pressure was fixed at 1 MPa during 8 s. Transparent solid samples were obtained with a good surface appearance and without injection defects (air bubbles inside the pieces, jetting, etc.).

2.3. Fabrication of Porous Samples. Production of porous materials was carried out by the solid state gas foaming process, in two high pressure vessels. One provided by TOP Industrie (Vaux Le Pénil, France), with a capacity of 300 cm^3 and maximum operation temperature and pressure of 250 °C and 40 MPa (400 bar), respectively. CO_2 pressure was supplied and controlled by an accurate pressure pump provided by Teledyne ISCO (Lincoln NE, U.S.). Another vessel is our self-designed vessel with glass windows and additional instrumentation (heaters, chillers, inner thermocouples, pressure control, control of the pressure release drop rate, etc.) with a capacity of 500 cm^3 and maximum operation temperature and pressure of 200 °C and 20 MPa, respectively.[31] This vessel also allows observation of different processes at controlled temperatures and pressures.

During the entire process, pressure and temperature inside the vessels were monitored.

Solid samples were introduced into the pressure vessel, under controlled CO_2 pressure and temperature during 24 h. Different pressures (from 7 to 30 MPa) and temperatures (from 10 to 70 °C) were used. After 24 h, samples were completely saturated by CO_2.[22] Then pressure was released, usually at pressure drop rates between 10 and 30 MPa/min with the TOP Industrie vessel, and between 1.4 and 45 MPa/min with the own-developed vessel. Porous structure was triggered during the pressure drop and stabilized at room temperature.

2.4. Characterization. Average molar masses of the MAM triblock copolymer were determined by Size Exclusion Chromatography (SEC) in a PL-GPC 50 Plus (Agilent Technologies) using THF (tetrahydrofuran) as a solvent with a polymer concentration of 3 mg/mL. Constant flow of 1.0 mL/min and a refraction index (RI) detector were employed. Calibration was made in THF with (homo)polystyrene calibration standards, being the molar mass values relative to the polystyrene standards.

Several characterization techniques were used in order to determine the main characteristics of the porous structure and the nanostructuration of the PMMA/MAM blends.

2.4.1. Porosity. Density of nanoporous and solid samples were determined by water-displacement method, based on Archimedes' principle. Porosity (or volume fraction of voids, V_f) was calculated from the relative density (obtained as the ratio between the density of the porous (ρ_f) and the solid (ρ_s) material) using eq 1.[33]

$$V_f = 1 - \frac{\rho_f}{\rho_s} \tag{1}$$

2.4.2. Scanning Electron Microscopy (SEM). Structure of nanoporous samples was studied using SEM (model Quanta 200FEG, FEI). Porous samples were immersed in liquid nitrogen and fractured to ensure that the microstructure remained intact. Surfaces were coated with gold using a sputter coater (model SCD 004, Balzers Union). The micrographs obtained were analyzed to measure the main pore size, pore density (N_v, pores per cubic centimeter in the porous material) and pore nucleation density (N_o, pore nucleation points per cubic centimeter of the solid material) with our developed specialized software based on FIJI/ImageJ.[32,33] The pore nucleation density can be calculated from the pore density and the porosity using eq 2.[24]

$$N_o = \frac{N_v}{1 - V_f} \tag{2}$$

This value represents the number of pores formed in a cubic centimeter of the solid material, assuming no coalescence between near pores during the stabilization of the porous structure. By comparison between the nucleation density (N_o) and the potential nucleation sites in the solid material (i.e., dispersed nanostructures), it is possible to analyze the efficiency of the nanodomains as nucleating agents (conversion ratio between potential nucleation sites and developed pores).

2.4.3. Atomic Force Microscopy (AFM). Solid samples were prepared by microtome to obtain flat surfaces with differences in height lower than 100 nm, which could be analyzed by AFM

dx.doi.org/10.1021/jp409803u | J. Phys. Chem. C 2014, 118, 4656−4663

(Multimode AFM, Veeco Instruments. WSxM software).[34] The AFM was operated in the amplitude modulation mode (tapping mode AFM).[35] Both the topography and the phase shift signal were recorded. The AFM phase images show a better contrast on polymer blends than the topography images because they detect changes in the energy dissipated by the AFM.[36] Over the AFM phase images obtained, it is possible to differentiate the poly(butyl acrylate) domains (black in the images) and the poly(methyl methacrylate) matrix (gray in the images). In the case of dispersed nanostructures, the volumetric density of nanodomains (nanodomains/cm^3) can be calculated from these images using eq 3.[24]

$$N_n = \left(\frac{n}{A}\right)^{3/2} \tag{3}$$

where n is the number of nanodomains observed in an AFM phase image, and A the area of the image in cm^2.

2.4.4. Transmission Electron Microscopy (TEM). Transmission Electron Microscopy is carried out at the Bordeaux Imaging Center (BIC, Université Bordeaux 2 Segalen). TEM observations on solid and porous samples were performed between 60 to 80 kV, at magnifications from x30 000 to x330 000, using a TEM microscope Hitachi H7650 with Orius camera. Thin cuts (60−70 nm) of the solid samples were obtained by a microtome carried out at −50 °C with a diamond knife. Then, cuts were deposited on Formvar copper grids and treated by a water solution with 2 wt % phosphotungstic acid (PTA) + 2 wt % benzyl alcohol. As reported in literature,[37−39] PTA staining contrasts butyl acrylate selectively (black in the images) and no or little PMMA (white or gray in the images).

In order to stiffen the foamed materials, filling of the voids by a TEM-contrasting liquid hardening formulation was attempted. A sol−gel organic−inorganic solution of several siloxane reactive monomers (formulation remains confidential and not publishable) allowed the voids to be filled without solubilization of the PMMA. The overall system gelifies and hardens rapidly (<30 min).

In the case of dispersed nanostructures, the volumetric density of core−shell nodules (core−shell nodules/cm^3) can be calculated from these images using eq 4.

$$N_n = \frac{n}{V} \tag{4}$$

where V is the volume of the sample in cm^3 (calculated from the area of the image and the thickness of the TEM sample), and n is the number of core−shell nodules observed in a TEM image. As the TEM image is a two-dimensional projection of the three-dimensional structure of the sample, some assumptions are needed to estimate the number of nanosized domains. Completely black structures in TEM images are assumed as core−shell structures completely contained in the sample and counted as units, and structures with a dark shell and gray core are assumed as core−shell nodules partially contained in the sample, because the gray core is due to the absence of the lower or upper part of the dark shell (not contained in the sample), and counted as halves.

2.4.5. CO_2 wt. % Uptake. CO_2 wt. % uptake by the polymer during saturation was measured for each sample by weighing the samples just after the pressure release.

3. RESULTS AND DISCUSSION

3.1. Self-Assembled Nanostructures in the Foam-Precursor Polymer Blends (PMMA/MAM). Self-assembling or nano structuration in polymer/block copolymer blends results from the microphase separation between different chemical blocks, which will act as a pattern for the porous structure.

3.1.1. Low Contents of MAM in PMMA. Each blend was analyzed from an injected bulk dense sample in two different planes, one containing the injection direction and another perpendicular to the injection direction.

TEM micrographs (only if samples are treated by phosphotungstic acid (PTA)) from 92.5-PMMA/7.5-MAM and 95-PMMA/5-MAM blends show regular well-dispersed nodules in the form of core−shell or micellar objects with a white PMMA core, and a black poly(butyl acrylate) (PBA) shell or layer, the apparent diameter of the objects is 20−25 nm (for generic example, see micrographs of Figure 1a). These nodules

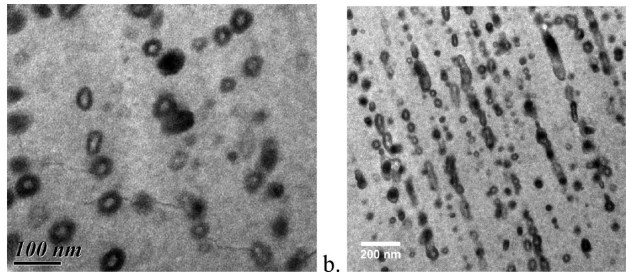

Figure 1. 90-PMMA/10-MAM blends (a) TEM micrograph, showing the core−shell structure of PBA domains. (b) TEM micrograph showing the alignment of the core−shell nodules.

are embedded in a "white" matrix (probably the PMMA matrix + the PMMA blocks) with no orientation effect.

90-PMMA/10-MAM blends have a very similar nodular appearance (Figure 1a). Due to the "ABA" structure of the MAM block copolymer, core−shell nodules might be constituted by 3 layers, the outer one (PMMA layer) is soluble in the matrix and is not contrasted by PTA. An apparent diameter of 30 nm is measured on TEM micrographs. The micrograph observation along the injection flow direction allows detection of a strong alignment effect (i.e., the presence of arrays or lines of core−shell nodules over several micrometers) (Figure 1b or Figure 2).

80-PMMA/20-MAM and 75-PMMA/25-MAM blends are still exhibiting nodular dispersed objects, analogous to the previous systems, although a more pronounced alignment effect is seen in Figure 2 (core−shell nodules become ellipsoids) and have a higher apparent diameter (30−50 nm).

As a conclusion, below 25 wt. % of MAM, all blends present nanosized micellar structures, with a clear orientation in the injection direction in 10, 20, and 25wt. % MAM blends. Both techniques, AFM and TEM, agree about the core−shell nodules size, from 20 nm in 5 wt. % MAM blends to 50 nm in 20 wt. % MAM blends.

3.1.2. High Contents of MAM in PMMA. A different structure is observed in blends with 75 wt.-% of MAM. AFM phase images show no influence of the injection process on the orientation of the nanostructure (Figure 3). AFM is not enough to determine clearly the morphology whereas TEM images show a cocontinuous nanostructuration with poorly defined lamella of 20−30 nm apparent thickness (Figure 3).

A *CO_2 saturation annealing* was carried out at 50 °C, 30 MPa, 24 h, then releasing the pressure extremely slowly (ΔP over 24 h) to prevent any foaming. Under this condition, the orientation sensitivity is erased and random curved lamellas develop all over the matrix, showing a completely volume-structured material; with the darker parts (PBA) having an apparent thickness larger than the annealed sample (i.e., the thickness of apparent dark + white parts of the lamella >90 nm).

dx.doi.org/10.1021/jp409803u | J. Phys. Chem. C 2014, 118, 4656−4663

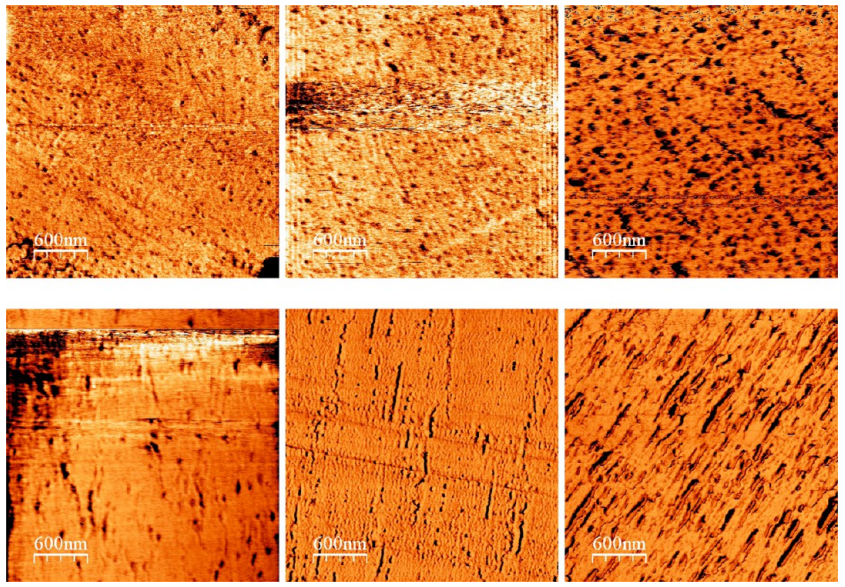

Figure 2. AFM phase images of PMMA/MAM blends 95/5 (left), 90/10 (middle), and 80/20 (right). Plane perpendicular to the injection direction (up) and plane containing the injection direction (down).

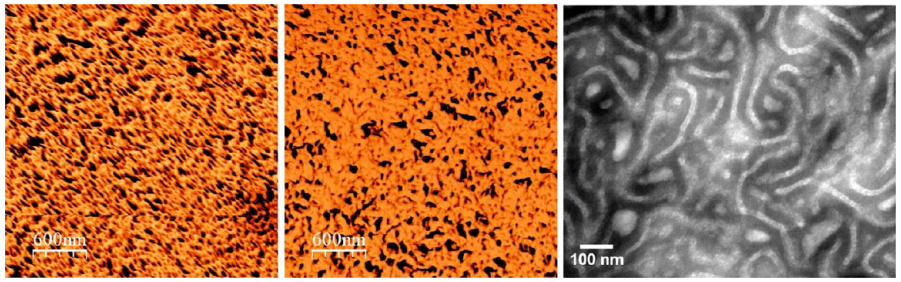

Figure 3. 25-PMMA/75-MAM blend. AFM phase image of the plane perpendicular to the injection direction (left), AFM phase image of the plane containing the injection direction (middle), and TEM image of PTA stained sample (right).

3.2. Porous Structures. The porous structures of the blends obtained by the solid state foaming process were analyzed by SEM. Pore formation by solid state gas foaming is usually governed by the process parameters, such as gas saturation pressure and temperature and pressure release drop rate;[24] however, PMMA/MAM blends could present a different behavior, with the nanostructure acting as a pattern for the porous structure.[22,23,40]

3.2.1. Low Contents of MAM in PMMA. Core−shell nodules in the solid blends have an appropriate size (20−50 nm) to act as nucleation sites of pores, i.e., higher than the critical nucleus radius (r^*) in a PMMA matrix, calculated using eq 5.[41]

$$r^* = 2t/P \tag{5}$$

where P is the saturation pressure, and t is the surface tension of PMMA (38.5 mN/m),[42] over the range of pressures of the study, 10−30 MPa, and r^* takes values between 2.5 and 8 nm. Porous structures were analyzed by SEM, obtaining an equivalent average value of the pore nucleation density (N_o) around 4.05×10^{14} nuclei/cm^3 for blends containing 5, 10, and 20 wt. %. Determination of the pore nucleation density was carried out from micrographs of the plane perpendicular to the injection direction, due to the fragility of the pore walls in the elongated pores fractured in the plane containing the injection direction (Figure 4 shows that the porous structure is missing when samples with highly elongated pores were fractured in that plane).

The value of the pore nucleation density (N_o) has the same order of magnitude and a quite similar value as the average core−shell nodules/nanodomain density (N_n) in these blends calculated from AFM images, $N_n^{AFM} = 4.43 \times 10^{14}$ nanodomains/cm^3,[40] and TEM images, $N_n^{TEM} = 5.30 \times 10^{14}$ nanodomains/cm^3.

Moreover, the shape of the porous structure can be analyzed in the same two planes as nanostructured dense samples, one containing the injection direction, and another perpendicular to the injection direction. Every sample presents pores with round shape in the plane perpendicular to the injection direction (Figure 4). But pores are clearly elongated in the injection direction (Figure 4) (10 and 20 wt. % of MAM). This corroborates the same previous observation in the dense precursor blends.

To ensure that the nucleation process is only or mainly governed by nanostructuration, it is needed to prove the decoupling of the process parameters, saturation pressure, and pressure release drop rate, from the nucleation process.

In a previous work, we found that saturation pressure (7 to 30 MPa) has no influence on porous structures working with these materials.[40] Here, the influence of the pressure release drop rate was characterized on samples of 90-PMMA/10-MAM, saturated at 7 MPa and room temperature, varying the pressure drop rate between 1.4 MPa/min to 45 MPa/min. Porous samples present a similar porous structure, and nucleation densities of 4×10^{14} and 3.75×10^{14} nuclei/cm^3 at drop rates of 45 and 1.4 MPa/min,

dx.doi.org/10.1021/jp409803u | J. Phys. Chem. C 2014, 118, 4656−4663

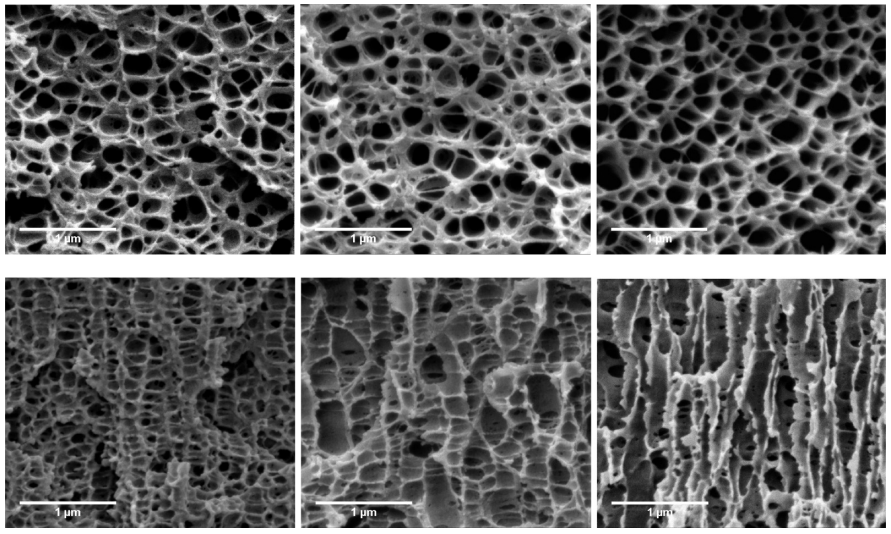

Figure 4. SEM images of porous PMMA/MAM blends 95/5 (left), 90/10 (middle), and 80/20 (right). Plane perpendicular to the injection direction (up) and plane containing the injection direction (down). Foaming conditions: 30 MPa, room temperature.

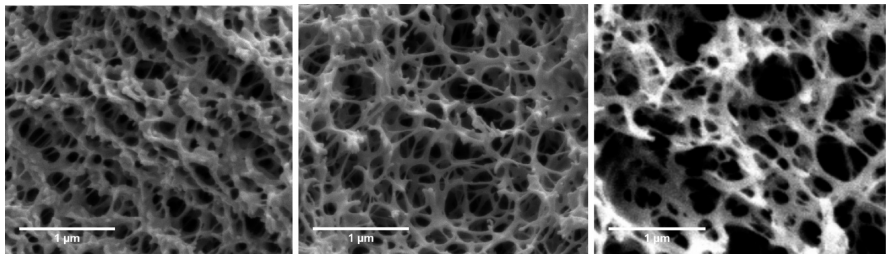

Figure 5. SEM images of porous 25-PMMA/75-MAM samples produced from saturation at 30 MPa and room temperature (left), 40 °C (middle), and 50 °C (right).

respectively. Thus, no influence of the pressure release drop rate on the nucleation process is found in the pressure drop rate range investigated.

So, a direct relationship between the solid blend nanostructuration (e.g., core−shell nodules density) and the porous structure (e.g., pore density) is found in porous samples of PMMA/MAM blends containing 5, 10, and 20 wt. % of MAM, whose expansion is triggered by pressure release from saturation pressures between 10 to 30 MPa and room temperature saturation.

3.2.2. High Contents of MAM in PMMA. SEM images from porous samples of 25-PMMA/75-MAM produced at 30 MPa and temperatures from 23 to 50 °C show a cocontinuous porous structure (Figure 5), with edges mainly of 20−40 nm thickness, comparable to the apparent thickness of lamella in the solid blends. Co-continuous porous structures are not individual pores, then no information about the nucleation process could be obtained from these structures.

A different approach is needed to prove a morphological relationship between the nanostructuration and the porous structure in blends with high contents of MAM.

Voids of the porous samples were attempted to be filled with a sol−gel organic−inorganic siloxane solution (see Experimental Section for details) in order to stiffen the material and reveal the Block Copolymer (BCP) location. As a result, the porous structure (light gray with black aggregates inside, coming from phase separation of the silica phase within the sol gel solution) could be differentiated from the polymer matrix (darker gray, without black aggregates) by the high contrast of a silica phase, which appears in the form of black aggregates, which are only present in the voids filled by the sol−gel organic−inorganic solution (Figure 6).

The porous structure in Figure 6 seems to reproduce the nanostructure of the 25-PMMA/75-MAM solid blend (Figure 3).

Nevertheless, a clear nanostructuration within the foams (i.e., pores + nanostructures, whatever the MAM content) cannot be evidenced by TEM so far, as though the core−shell nodules or the lamella had been blown up.

As a conclusion, nanostructuration of PMMA/MAM blends is the pattern of the porous structures obtained by gas dissolution foaming, both for low and high MAM contents. The higher CO_2-philty of PBA (compared to PMMA), and the difference between their glass transition temperatures (T_g), −50 °C for PBA, 110 °C for PMMA, promotes that nucleation only happens in the nanostructures, particularly in the PBA phase. It should be noticed that the PBA shell of the core−shell nodules or the PBA lamellae present appropriate sizes for the nucleation process taking place inside them. PBA presents a surface tension of 33.7 mN/m,[43] thus, from eq 5, it is obtained that r^* takes values from 2.2 to 6.7 nm in the range of pressures used to produce these foams.

After the nucleation process, the CO_2-swollen PMMA matrix allows growth of the porous structure, because the PMMA-CO_2 system is in the rubbery state even at low temperatures.[44,45] However, the small thickness of the PMMA walls and edges (a few nanometers) allows for rapid CO_2 desorption. As a consequence, PMMA enters the glassy state and constrains growth of the porous structure in the PBA phase, preventing coalescence of the pores.

dx.doi.org/10.1021/jp409803u | J. Phys. Chem. C 2014, 118, 4656−4663

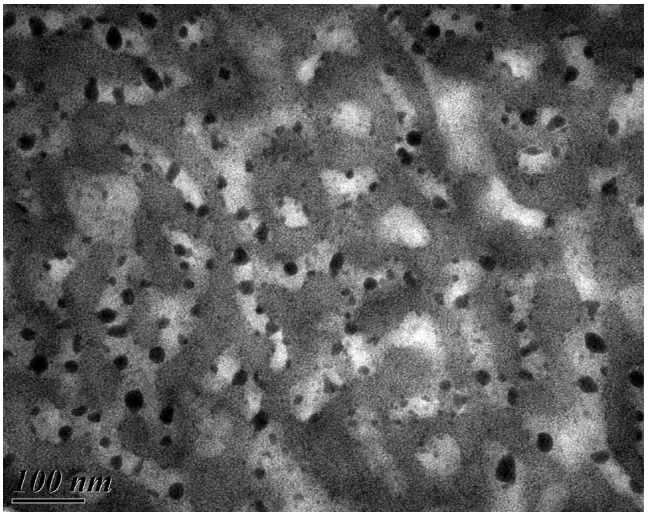

Figure 6. TEM image of "filled" porous 25-PMMA/75-MAM sample.

Influence of the core−shell morphology on the morphology of the pores cannot be strictly determined from the previous results. However, if the critical nucleation radius of the PBA phase is smaller than the size of the PMMA core of the dispersed copolymer objects, then the core can act as a nucleation point inside the PBA phase.

3.3. Control of Porosity and Average Pore Size.

Influence of blend composition and process parameters (saturation pressure and temperature) on the nucleation and morphology of the porous structure have been previously determined. Now, their influence on the pore growing is discussed.

3.3.1. Low Contents of MAM in PMMA. PMMA/MAM injected blends containing 10 and 20 wt. % of MAM were selected to produce porous structures that could be potentially used as membranes. Oriented nanostructuration of these materials acting as a pattern allows one to obtain elongated pores with a clear orientation.

Porous materials were produced after saturation at 30 MPa and room temperature from the selected blends, and also 95-PMMA/5-MAM blend, to study the influence of the MAM content on the porosity of the samples and their pore size (Figure 4). Direct relationships between the pore size and porosity evolution are expected due to the constant pore nucleation density previously mentioned.

Pore size was determined from the images obtained in the plane perpendicular to the injection direction, because this size will be the effective pore size to filtration processes.

First, for given processing parameters (pressure and temperature), the results show that pore size and porosity are increased with the amount of MAM (Figure 7), the increment in diameter and porosity is however small, $V_f = 0.53$ to 0.58, $\phi = 170$ to 190 nm. We expect that this is due to the higher CO_2 sorption related to the MAM content.

Second, influence of the saturation pressure on porosity and pore size, was analyzed on samples of 90-PMMA/10-MAM produced at room temperature and increasing pressures between 10 and 30 MPa (Figure 8). As expected, pore size and porosity grow in parallel, but an asymptotic behavior seems to be reached at high pressures (especially for porosity), giving a further justification of the nucleation and gas location role of the PBA blocks.

This parallel behavior of pore size and porosity can be explained from the constant nucleation density controlled by the

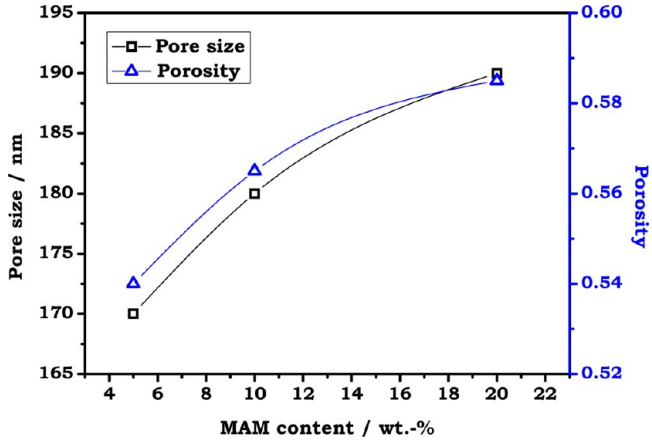

Figure 7. Effect of MAM content on the porosity and pore size in low MAM content blend porous materials. Foaming conditions: 30 MPa and room temperature.

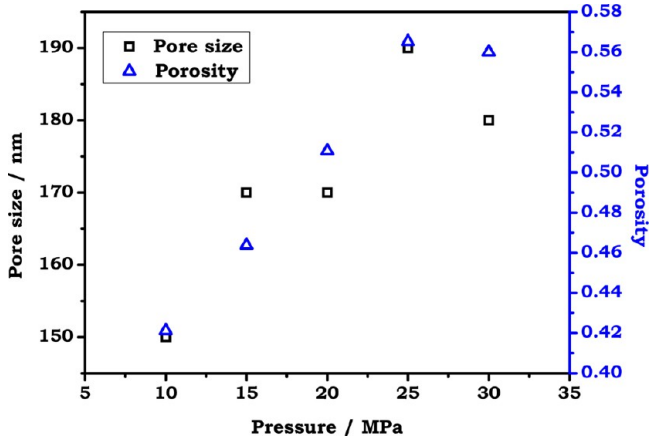

Figure 8. Effect of saturation pressure on the porosity and pore size in 90-PMMA/10-MAM porous blends. Saturation carried out at room temperature.

nanostructuration of these materials. The pore nucleation density of 90-PMMA/10-MAM blends produced from 10 to 30 MPa is nearly constant, with values between 3.68×10^{14} and 4.16×10^{14}.

Adding measurements of the CO_2 uptake of the polymer blends during the saturation process were carried out to improve the understanding of the results obtained (Figure 9). As expected, CO_2 uptake presents a direct linear relationship with the saturation pressure. Therefore, the increment of pore size with the saturation pressure is due to the higher internal pressure after the external pressure release, and the plasticization of the PMMA matrix.[44,45]

Thus, porous structures with the same morphology and different pore size and porosity could be obtained. Pore size and porosity are controlled by the amount of MAM or by the saturation pressure during the production process.

These porous structures are produced in bulk, membranes of 60−100 nm thickness could be obtained using microtome at low temperatures. The membrane thickness is limited by the pore size in the injection direction, being probably too thin to support the pressure gradients needed for the filtration process without a structural failure. The use of a backside support with large openings could avoid this limitation and allow the use of these membranes in filtration processes.[46]

dx.doi.org/10.1021/jp409803u | J. Phys. Chem. C 2014, 118, 4656−4663

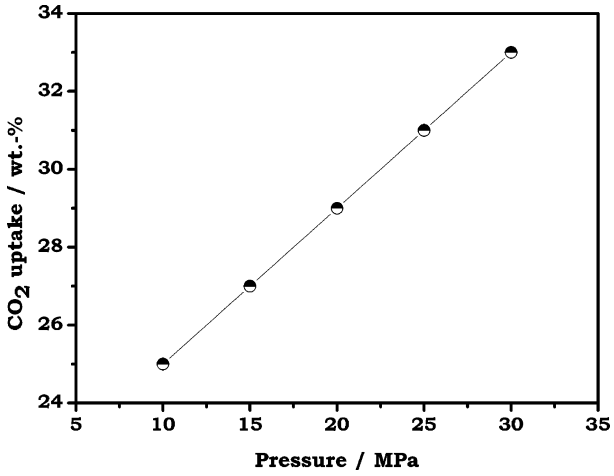

Figure 9. Relationship between the CO_2 saturation pressure and the CO_2 uptake for 90-PMMA/10-MAM samples.

3.3.2. High Contents of MAM in PMMA. As explained before, porous samples produced from the 25-PMMA/75-MAM blend allow a cocontinuous open porous structure to be obtained, which could be used as a depth filter.

Porous samples from this blend were produced at 30 MPa and temperatures between room temperature and 70 °C, in order to analyze the effect of the process temperature on the porosity of the samples, and the pore size (pore size means in this case the average size of the channels of the cocontinuous porous structure). Samples produced at 60 and 70 °C are discarded, due to the absence of the nanopores at these elaboration temperatures.

Morphologies of foamed samples produced between room temperature and 50 °C were given in Figure 5, while effect of CO_2 saturation temperature on the porosity and pore size in the 25-PMMA/75-MAM porous blends is shown in Figure 10.

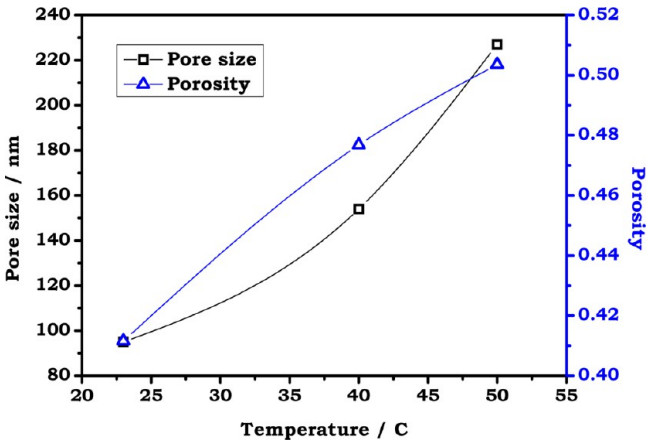

Figure 10. Effect of CO_2 saturation temperature on the porosity and pore size in 25-PMMA/75-MAM porous materials, saturation pressure = 30 MPa.

It is proven that (nano) pore size and porosity can be controlled by the process temperature, at temperatures up to 50 °C. Porosity of 25-PMMA/75-MAM blend foams present a lower variation than expected with temperature saturation (since porosity of neat MAM foams changes between 0.5 to 0.2 in the same temperature range), while the pore size increases, which implies that the increment of the pore size is mainly due to coalescence between pores and not due to a higher expansion of the polymeric matrix.

These structures are also produced in bulk, the thickness of the samples to be used on filtration can be controlled by the thickness of the solid samples (taking into account the sample's expansion during the process), or just by cutting the bulk samples to the appropriate thickness. Then, preparation of filters from PMMA/MAM blends with high amounts of MAM can be simpler than from blends with low amounts of MAM. Also, these cocontinuous pore structures present the advantage that pore clogging will not be as severe as in a structure with well-defined closed pores, due to the high interconnection of the pores.

4. CONCLUSIONS

A route to produce nanoporous structures, which could be used in filtration processes, has been presented. This route presents several advantages: it is based on an environmentally friendly process, the solid state foaming by CO_2; this process is industrially scalable; the same route allows obtaining both membranes and depth filters. If the main component of the polymer matrix is PMMA in the presence of an adequate block copolymer (here MAM), then it presents a proven biocompatibility; and characteristics of the porous structures, such as the porosity and pore size, can be adjusted by composition and the process parameters.

This method is based on the particular behavior of nanostructured PMMA/MAM blends under the solid state foaming process. It has been demonstrated that nanoporous materials with pore sizes between 100 and 200 nm can be produced by a gas foaming process from PMMA/MAM blends. These materials present the unique characteristic that the pore nucleation process is controlled mainly by the nanostructure morphology of the initial solid blends.

Porous material morphology is governed by nanostructure, whereas process parameters control the overall porosity and the average pore size.

Further investigation on these PMMA/MAM systems, or other block copolymers with similar characteristics, could open a new way of fabrication of tunable nanoporous structures for microfiltration processes.

AUTHOR INFORMATION

Corresponding Author

*Phone: +34 983 423572; e-mail: jpinto@fmc.uva.es (J.P.), marrod@fmc.uva.es (M.A.R.-P.).

Notes

The authors declare no competing financial interest.

ACKNOWLEDGMENTS

Financial assistance from MCINN (MAT2009-14001-C02-01 and MAT2012-34901), Junta of Castile and Leon (VA174A12-2 and VA035U13) and FPU grant AP2008-03603 (J.P.) from the Spanish Ministry of Education is gratefully acknowledged. The help and expertise of Dr. Etienne Gontier, Dr. Soizic Lacampagne, and Dr. Melina Petrel (BIC, Université Bordeaux Segalen) is acknowledged for TEM observations and samples preparation.

REFERENCES

(1) Schafer, A. I.; Davey, J. Appropriate Technologies for Environmental Protection in the Developing World; Springer Science and Business Media B.V.: Edinburgh, U.K., 2009.

(2) Eds: Nunes, S.; Peinemann, K.-V. *Membrane Technology in the Chemical Industry*; Wiley−VCH: Weinheim, Germany, 2001.
(3) Ulbricht, M. Advanced Functional Polymer Membranes. *Polymer* **2006**, *47*, 2217−2262.
(4) Yigzaw, Y.; Piper, R.; Tran, M.; Shukla, A. A. Exploitation of the Adsorptive Properties of Depth Filters for Host Cell Protein Removal during Monoclonal Antibody Purification. *Biotechnol. Prog.* **2006**, *22*, 288−296.
(5) Li, L.; Schulte, L.; Clausen, L. D.; Hansen, K. M.; Jonsson, G. E.; Ndoni, S. Gyroid Nanoporous Membranes with Tunable Permeability. *ACS Nano* **2011**, *5*, 7754−7766.
(6) Madou, M. J.; *Fundamentals of Microfabrication*, 2nd ed.; CRC Press: Boca Raton, FL, 2002.
(7) Hillmyer, M. A. Nanoporous Materials from Block Copolymers Precursors. *Adv. Polym. Sci.* **2005**, *190*, 137−181.
(8) Mehta, A.; Zydney, A. L. Permability and Selectivity Analysis for Ultrafiltration Membranes. *J. Membr. Sci.* **2005**, *249*, 245−249.
(9) Akthakul, A.; McDonald, W. F.; Mayes, A. M. Noncircular Pores on the Surface of Asymmetric Polymer Membranes: Evidence of Pore Formation via Spinodal Demixing. *J. Membr. Sci.* **2002**, *208*, 147−155.
(10) Krause, B.; Diekmann, K.; van der Vegt, N. F. A.; Wessling, M. Open Nanoporous Morphologies from Polymeric Blends by Carbon Dioxide Foaming. *Macromolecules* **2002**, *35*, 1738−1745.
(11) Sara, M.; Sleytr, U. B. S-Layer Proteins. *J. Bacteriol.* **2000**, *182*, 859−868.
(12) Kamide, K.; *Cellulose and Cellulose Derivatives*; Elsevier Science: Amsterdam, Netherlands, 2005.
(13) Hedrick, J. L.; Miller, R. D.; Hawker, C. J.; Carter, K. R.; Volksen, W.; Yoon, D. Y.; Trollsas, M. Templating Nanoporosity in Thin-Film Dielectric Insulators. *Adv. Mater.* **1998**, *10*, 1049−1053.
(14) Hentze, H.-P.; Antonietti, M. Porous Polymers and Resins for Biotechnological and Biomedical Applications. *Rev. Mol. Biotechnol.* **2002**, *90*, 27−53.
(15) Hentze, H.-P.; Antonietti, M. Template Synthesis of Porous Organic Polymers. *Curr. Opin. Solid State Mater. Sci.* **2001**, *5*, 343−353.
(16) Jacson, E. A.; Hillmyer, M. A. Nanoporous Membranes Derived from Block Copolymers: From Drug Delivery to Water Filtration. *ACS Nano* **2010**, *4* (7), 3548−3553.
(17) Lazzari, M.; Lopez-Quintela, M. A. Block Copolymers as a Tool for Nanomaterial Fabrication. *Adv. Mater.* **2003**, *15* (19), 1583−1594.
(18) Park, C.; Yoon, J.; Thomas, E. L. Enabling Nanotechnology with Self Assembled Block Copolymer Patterns. *Polymer* **2003**, *44*, 6725−6760.
(19) Smarsly, B.; Xomeritakis, G.; Yu, K.; Liu, N.; Fan, H.; Assink, R. A.; Drewien, C. A.; Ruland, W.; Brinker, C. J. Microstructural Characterization of Polystyrene-block-ply(ethylene oxide)-Templated Silica Films with Cubic-Ordered Spherical Mesopores. *Langmuir* **2003**, *19*, 7285−7301.
(20) Li, L.; Yokoyama, H.; Nemoto, T.; Sugiyama, K. Facile Fabrication of Nanocellular Block Copolymer Thin Films using Supercritical Carbon Dioxide. *Adv. Mater.* **2004**, *16*, 1226−1229.
(21) Yokoyama, H.; Li, L.; Sugiyama, K.; Nemoto, T. Tunable Nanocellular Polymeric Monoliths using Fluorinated Block Copolymer Templates and Supercritical Carbon Dioxide. *Adv. Mater.* **2004**, *16*, 1542−1546.
(22) Reglero-Ruiz, J. A.; Pedros, M.; Tallon, J.-M.; Dumon, M. Micro and Nano Cellular Amorphous Polymers (PMMA, PS) in Supercritical CO_2 Assisted by Nanostructured CO_2-Philic Block Copolymers—One Step Foaming Process. *J. Supercrit. Fluid.* **2011**, *58*, 168−176.
(23) Dumon, M.; Reglero-Ruiz, J. A.; Pinto, J.; Rodriguez-Perez, M. A.; Tallon, J. M.; Pedros, M.; Viot, P. Block Copolymer-Assisted Microcellular Supercritical CO_2 Foaming of Polymers and Blends. *Cell. Polym.* **2012**, *31*, 207−222.
(24) Kumar, V.; Suh, N. P. A Process for making Microcellular Thermoplastic Parts. *Polym. Eng. Sci.* **1990**, *30*, 1323−1329.
(25) Jacobs, L. J. M.; Kemmere, M. F.; Keurentjes, J. T. F. Sustainable Polymer Foaming using High Pressure Carbon Dioxide: A Review on Fundamentals, Processes and Applications. *Green Chem.* **2008**, *10*, 731−738.
(26) Wells, S. L.; DeSimone, J. CO_2 Technology Platform: An Important Tool for Environmental Problem Solving. *Angew. Chem., Int. Ed.* **2001**, *40*, 518−527.
(27) Hollick, E. J.; Spalton, D. J.; Ursell, P. G.; Pande, M. V. Biocompatibility of Poly(methyl methacrylate), Silicone, and AcrySof Intraocular Lenses: Randomized Comparison of the Cellular Reaction on the Anterior Lens Surface. *J. Cataract Refr. Surg.* **1998**, *24*, 361−366.
(28) Hakim, R. M.; Fearon, D. T.; Lazarus, J. M. Biocompatibility of Dyalisis Membranes: Effects of Chronic Complement Activation. *Kidney Int.* **1984**, *26*, 194−200.
(29) Lalande, L.; Plummer, C. J. G.; Manson, J.-A. E.; Gerard, P. The Influence of Matrix Modification on Fracture Mechanisms in Rubber Toughened Polymethylmethacrylate. *Polymer* **2006**, *47*, 2389−2401.
(30) Lalande, L.; Plummer, C. J. G.; Manson, J.-A. E.; Gerard, P. Microdeformation Mechanisms in Rubber Toughened PMMA and PMMA-based Copolymers. *Eng. Fract. Mech.* **2006**, *73*, 2413−2426.
(31) Solórzano, E.; Escudero, J.; Pinto, J.; Rodriguez-Perez, M. A.; de Saja, J. A.Evolution of Polymers during the Gas Dissolution Process. In *Proceedings International Conference on Diffusion in Solids and Liquids* ; Algarve, Portugal, 2011.
(32) Abramoff, M. D.; Magelhaes, P. J.; Ram, S. J. Image Processing with ImageJ. *Biophotonics Int.* **2004**, *11*, 36−42.
(33) Pinto, J.; Solorzano, E.; Rodriguez-Perez, M. A.; de Saja, J. A. Characterization of the Cellular Structure based on User-Interactive Image Analysis Procedures. *J. Cell. Polym.* **2013**, *49*, 555−575.
(34) Horcas, I.; Fernandez, R.; Gomez-Rodriguez, J. M.; Colchero, J.; Gomez-Herrero, J.; Baro, A. M. WSXM: A Software for Scanning Probe Microscopy and a Tool for Nanotechnology. *Rev. Sci. Instrum.* **2007**, 78 DOI: 10.1063/1.2432410.
(35) Garcia, R.; San Paulo, A. Attractive and Repulsive Tip-Sample Interaction Regimes in Tapping-Mode Atomic Force Microscopy. *Phys. Rev. B* **1999**, *60*, 4961−4967.
(36) García, R.; Gómez, C. J.; Martinez, N. F.; Patil, S.; Dietz, C.; Magerle, R. Identification of Nanoscale Dissipation Processes by Dynamic Atomic Force Microscopy. *Phys. Rev. Lett.* **2006**, *97*, 016103.
(37) Lalande, L. *Structure et Mecanismes de Microdeformation de Polymethylmethacrylates Renforces au Choc*; Ph. D. dissertation, Ecole Polytechnique Federale de Laussanne: France, 2007.
(38) Chen, W.; Zhu, M.; Song, S.; Sun, B.; Chen, Y.; Adler, J. H. Morphological Characterization of PMMA/PAN Composite Particles in Nano to Submicro Size. *Macromol. Mater. Eng.* **2005**, *290*, 669−674.
(39) Gallego Ferrer, G.; Salmeron Sanchez, M.; Gómez Ribelles, J. L.; Romero Colomer, F. J.; Monleón Pradas, M. Nanodomains in a Hydrophilic-Hydrophobic IPN base don Poly(2-hydroxyethyl acrylate) and Poly(ethyl acrylate). *Eur. Polym. J.* **2007**, *43*, 3136−3145.
(40) Pinto, J.; Dumon, M.; Pedros, M.; Reglero, J.; Rodriguez-Perez, M. A. Nanocellular CO_2 Foaming of PMMA Assisted by Block Copolymer Nanostructuration. *Chem. Eng. J.* **2014**, *243C*, 428−435.
(41) Spitael, P.; Macosko, C. W.; McClurg, R. B. Block Copolymer Micelles for Nucleation of the Microcellular Thermoplastic Foams. *Macromolecules* **2004**, *37* (7), 6874−6882.
(42) Kwok, D. Y.; Leung, A.; Lam, C. N. C.; Li, A.; Wu, R.; Neumann, A. W. Low-Rate Dynamic Contact Angles on Poly(methyl methacrylate) and the Determination of Solid Surface Tensions. *J. Colloid Interface Sci.* **1998**, *206*, 44.
(43) Mark, J. E. *Physical Properties of Polymers Handbook*, 2nd ed.; Springer Science-Business Media, LLC: New York, 2007.
(44) Goel, S. K.; Beckman, E. J. Generation of Microcellular Polymers using Supercritical CO_2. *Cell. Polym.* **1993**, *12*, 251−274.
(45) Nawaby, A. V.; Handa, Y. P.; Liao, X.; Yoshitaka, Y.; Tomohiro, M. Polymer-CO_2 Systems Exhibiting Retrograde Behavior and Formation of Nanofoams. *Polym. Int.* **2007**, *56*, 67−73.
(46) Warkiani, M. E.; Lou, C.-P.; Gong, H.-Q. Fabrication and Characterization of a Microporous Polymeric Micro-filter for Isolation of *Cryptosporidium parvum* oocysts. *J. Micromech. Microeng.* **2011**, 21 DOI: 10.1088/0960-1317/21/3/035002.